Stereo Plume Height and Motion Retrievals for the Record-Setting Hunga Tonga-Hunga Ha'apai Eruption of 15 January 2022

J. L. Carr[1*], Ákos Horváth[2], Dong L. Wu[3], and Mariel D. Friberg[3,4]

[1]Carr Astronautics, Greenbelt, MD USA.

[2]Meteorological Institute, Universität Hamburg, Hamburg, Germany.

[3]NASA Goddard Space Flight Center, Greenbelt, MD USA.

[4]University of Maryland, College Park, MD USA.

Corresponding author: James Carr (jcarr@carrastro.com)

*6404 Ivy Lane, Suite 333, Greenbelt, MD 20770 USA.

Key Points:

- The Hunga Tonga-Hunga Ha'apai eruption of 15 January 2022, lofted material above 30 km to record-breaking heights of ~55 km.
- Our stereo-winds code retrieved height and motion vectors from GOES-17 and Himawari-8 every 10 minutes immediately after the event.
- Radio Occultation bending angles confirm plume altitudes.

Abstract

Stereo methods using GOES-17 and Himawari-8 applied to the Hunga Tonga-Hunga Ha'apai volcanic plume on 15 January 2022 show overshooting tops reaching 50-55 km altitude, a record in the satellite era. Plume height is important to understand dispersal and transport in the stratosphere and climate impacts. Stereo methods, using geostationary satellite pairs, offer the ability to accurately capture the evolution of plume top morphology quasi-continuously over long periods. Manual photogrammetry estimates plume height during the most dynamic early phase of the eruption and a fully automated algorithm retrieves both plume height and advection every 10 minutes during a more frequently sampled and stable phase beginning three hours after the eruption. Stereo heights are confirmed with Global Navigation Satellite System Radio Occultation (GNSS-RO) bending angles, showing that most of the plume was lofted 30–40 km into the atmosphere. Cold bubbles are observed in the stratosphere with brightness temperature of ~173K.

Plain Language Summary

The Hunga Tonga-Hunga Ha'apai volcano in the South Pacific erupted violently on January 15, 2022. A volcanic plume from the eruption was lofted into the stratosphere to altitudes that are unprecedented in the era of satellite observations. We observed the highest part of the plume at 55 km and tracked the motion of the plume in 3D in the vicinity of the volcano for a seven-hour period, every 10 minutes, using imagery from the geostationary GOES-17 and Himawari-8 satellites that are positioned at different locations on the equator. The apparent shift in the plume as seen from two different vantage points contains information about the plume height and the apparent movement of the plume as it is repeatedly observed by one satellite contains information about the plume velocity. We confirmed our height observations using radio occultation measurements that NOAA uses to profile the atmosphere. Radio waves are normally bent as they pass through the atmosphere from satellite to satellite, nearly grazing the Earth's surface, but when radio waves pass through the volcanic plume, there is an anomalously large change in bending angle.

1 Introduction

The Hunga Tonga-Hunga Ha'apai eruptions of January 2022 culminated in a dramatic event on 15 January 2022. The plume from this underwater eruption was captured in imagery from the geostationary GOES-17 and Himawari-8 satellites beginning just after 04:00Z. Applying stereo methods to this imagery, we show that the 15 January 2022 eruption lofted a volcanic plume well above the tropopause and into the stratosphere, with the highest overshooting tops reaching altitudes of 50–55 km, a record in the satellite era. Determining the height of volcanic plumes has an important implication for their dispersion and transport in the atmosphere as well as their lifetime impacts on Earth's climate. Although other observational techniques exist to estimate volcanic plume heights, including the temperature method, LiDAR (e.g., CALIOP), and UV limb sounding (e.g., OMPS), only stereo methods using geostationary satellite pairs offer the ability to accurately capture the evolution of plume top morphology quasi-continuously over long periods. We use manual photogrammetry to estimate plume height during the most dynamic early phase of the eruption and a fully automated algorithm to retrieve both plume height and advection every 10 minutes during a more frequently sampled and stable phase beginning three hours after the eruption. Global Navigation Satellite System Radio

Occultation (GNSS-RO) bending angles similarly show that the bulk of the plume was lofted 30–40 km into the atmosphere.

2 Materials and Methods

We rely on stereo methods previously developed at NASA for tracking wind tracers from multiple satellites ("stereo winds"). These tools have already been applied to stereo observations from Himawari-8 and MODIS of the 2019 eruption of Raikoke (Horváth et al., 2021a and 2021b). The stereo-winds code for a geostationary pair is fully described in Carr et al. (2020). It offers the ability to retrieve both the height and the motion of a volcanic plume automatically and nearly continuously until the eruption dies down and the plume becomes too tenuous to track effectively. A similar approach has been applied to the study of an eruption of Mt. Etna in 2013 using a pair of Meteosat satellites (Merucci et al., 2016).

We use geostationary satellite imagery from GOES-17 nominally stationed at 137.2°W and Himawari-8 nominally stationed at 140.7°E. Both satellites have nearly identical 16-channel imagers and capture the Earth's Full Disk (FD) every 10 minutes. Both imagers have similar capabilities to acquire smaller sectors with shorter refresh times. In particular, GOES can acquire an approximately 1000×1000 km^2 Mesoscale (MESO) scene every 1 minute. NOAA centered a MESO scene over the eruption at 07:05Z to begin covering the volcano every minute. Before 07:05Z, the volcano was only covered in the FD scenes repeating every 10 minutes. Stereo-winds feature tracking works better when the time between scene repetitions is shorter. At the beginning of this eruption, as the radius of the plume top expanded at a mean radial speed of ~50 m s^{-1} from ~20 km at 04:10Z to ~55 km at 04:20Z and to ~80 km at 04:30Z, features that otherwise could be tracked morphed quickly in the billowing and rapidly expanding plume. This made automated feature tracking more difficult using the 10-minute GOES-17 FD scenes. Therefore, we focused our use of the stereo-winds code on GOES-17 MESO scenes paired with a single near-simultaneous Himawari FD and used manual photogrammetry (stereo and shadow analysis) with FD pairs before 07:05Z. For example, the Himawari FD beginning at 07:00Z, starts above the North Pole and progresses towards the south, reaching the volcano around 07:06Z; therefore, we pair GOES MESO scenes at 07:05Z, 07:06Z, and 07:07Z with the single 07:00Z Himawari FD scene. This pattern repeats every 10 minutes. The sun has already set at the volcanic site by 07:00Z, so we use the long-wave Band 14 (B14) with a center wavelength at 11.2 μm and spatial resolution of 2 km for both satellites.

Simultaneous stereo pairs are not required by the stereo-winds code as pixel acquisition times are used in the retrieval model. In our case, the 07:06Z GOES-17 MESO and the 07:00Z Himawari FD differ from exact simultaneity by either ~10 s, ~40 s, or ~70 s across the mesoscale domain depending on which of the three 30-s swaths of the Himawari FD that cover the mesoscale domain contain the pixel. The apparent displacement of a feature between images represents a combination of motion and geometric parallax that the model separates knowing the pixel times.

Our manual photogrammetry relies on the highest resolution (0.5 km) GOES and Himawari red band (0.64 μm) FD pairs with a typical non-simultaneity of ~30 s in each 10-minute slot. Prata and Grant (2001) and Horváth et al. (2021a) give a detailed description of the method. In short, the height of a feature visually matched in the two images is determined from the ellipsoid-projected parallax between the match points and the corresponding satellite view/azimuth angles. The method can also be applied to apparent shadows observed in a single

image. The second satellite view is effectively replaced by the solar-projected location of the feature, i.e., the shadow terminus. Note that the method can estimate the height but not the motion of a feature. The shadow variant has the advantage of only requiring a single image. Still, sampling is limited to shadowed areas, and it can be challenging to pinpoint the exact location of the shadow terminus due to the blurring effect of a penumbra.

Manual feature matching between two satellite images of the plume is relatively straightforward; however, the horizontal and vertical motion of the feature introduces a height error due to any non-simultaneity between views. In our case, the GOES-17 and Himawari-8 view zenith/azimuth angles are around 50º/66º and 55º/-71º, respectively. This stereo geometry leads to a parallax almost precisely in the east-west direction, and a height error of ~0.4 km for every 1 km parallax error (see Eq. 8 in Horváth et al., 2021a)—the corresponding height error sensitivity for our shadow geometry is ~0.3 km per 1 km parallax. In the early phases of the eruption, the velocity of the fastest moving plume element is ~50 m s^{-1} in both the horizontal and vertical directions. During the 30 s between the satellite views, this results in a ~1.5 km horizontal movement and a ~1.5 km vertical rise, the latter of which translates to a ~3.7 km parallax increase. In the worst case, when these motion parallax errors add up, the total parallax error is ~5.2 km, amounting to a ~2 km height overestimation. Vertical velocity can be negative (but smaller in magnitude) when overshooting tops collapse. There can also be partial cancellation between the motion parallax errors, depending on the direction of the horizontal velocity. Therefore, a ±2 km height uncertainty is expected for the most dynamic plume features (although overestimation is more likely than underestimation), which is acceptable considering the extreme heights encountered. Both manual photogrammetry and stereo-winds methods are most accurate when the motion is predominantly perpendicular to the local vertical and stereo pairings are nearly simultaneous.

3 Results

3.1 Manual Photogrammetry

Figure 1 shows the maximum height estimates found at 04:30Z. The plume resembled a stack of pancakes with several identifiable layers, capped by a large central dome (see the contrast-enhanced Supplementary Exhibit S1). Heights were calculated for thirty plume retrievals and one low-level cloud at 2 km altitude serving as a reference. The stereo retrievals indicate layers at 20–21 km, 26–27 km, and the massive topmost ring of ~80 km radius at 38–40 km. There are significant km-scale variations within this rugged topmost ring, demonstrating the sheer dynamism of the explosive rise. Most remarkably, the central dome reached an altitude of ~55 km. The retrievals show a systematic increase in height as sampling ascends from the base to the dome's peak. A rough estimate of peak height from applying the side view method of Horváth et al. (2021a) to the corresponding GEO-KOMPSAT-2A image is in Supplementary Exhibit S2. The GOES-17 view was favorable for applying the shadow method and is unaffected by motion effects. The long white arrow marks the apparent shadow of a local peak in the topmost ring, cast on the ocean surface. For a solar zenith/azimuth angle of 68º/-108º, the 145.7 km shadow length corresponds to a plume edge height of ~40 km, in good agreement with the nearby GOES-17–Himawari-8 stereo estimates. The shorter white arrow indicates the shadow of a dome feature cast on the ring. This 61.7 km long shadow corresponds to an ~18 km height differential relative to the ~38 km altitude of the ring feature at the shadow terminus, consistent

with a peak dome altitude of ~55 km within the expected tolerance of ±2 km. Shadow-based plume height estimates for the 04:50–05:00Z time slots are also in Supplementary Exhibit S3.

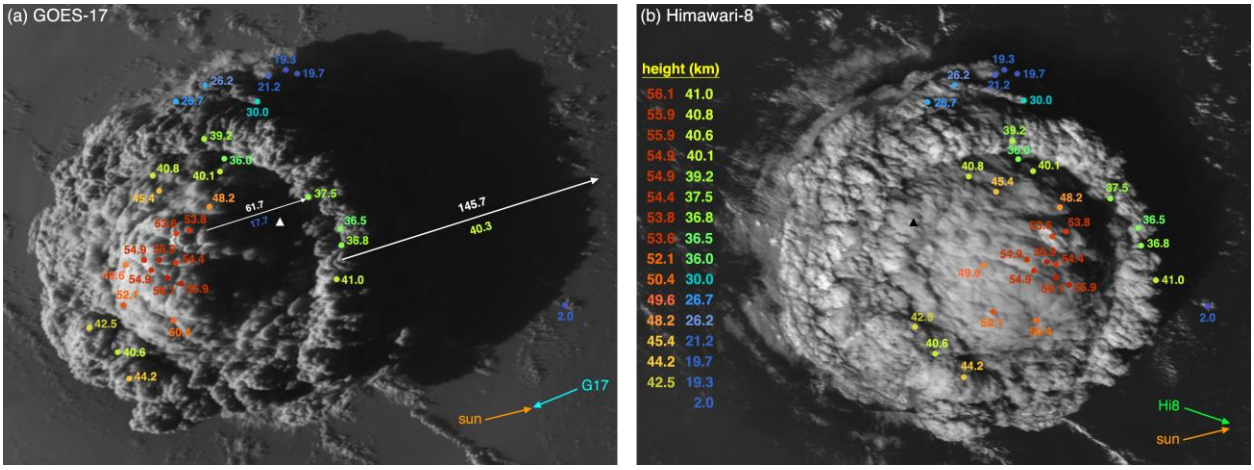

Figure 1. Image of the plume on 15 January 2022 at 04:30Z from (a) GOES-17 and (b) Himawari-8. Colored dots mark manual stereo height estimates (in km), and the triangle shows the volcano's location. The white arrows in panel (a) depict the shadow of a plume edge feature and a dome feature, with the shadow length and the derived height given above/below the arrow. Arrows in the lower right of each panel indicate the sun-to-pixel and satellite-to-pixel azimuths.

3.2 Automated Stereo-Winds Method

The stereo-winds method was applied after 07:05Z when NOAA placed the GOES-17 MESO1 scene on the volcano. The 1-minute cadence of the MESO scenes is nearly ideal as it allows enough time for motion to be observed but leaves feature shapes sufficiently invariant to be accurately tracked with subpixel precision. Figure 2a shows the jointly retrieved stereo heights, and advection vectors for 08:06Z (uses GOES-17 MESO scenes at 08:05Z, 08:06Z, 08:07Z) paired with the Himawari 08:00Z FD. Smaller tracking templates allow for a higher resolution characterization of the plume geometry and dynamics, but this must be balanced against tracking accuracy. We selected 16x16 pixel templates (32 km feature spatial resolution) and oversampled the scene 4:1 (8 km sampling). A lofted stratospheric plume mostly above 30 km is seen over a lower cold umbrella at ~18 km near the tropopause. The expansion and westward drift of the plume is evident from the advection vectors. Accompanying temperature assignments have been made according to the Effective Blackbody Temperature (EBBT) of the tracking templates taken from the 08:06Z MESO scene. Templates lower than 22 km (cold umbrella and troposphere) are presumed to be cold targets over warmer backgrounds and are assigned the mean temperature of the 20% coldest pixels. Templates 22 km and above are expected to be warmer than the cold umbrella and are assigned the mean temperature of the 20% warmest pixels because of the negative stratospheric lapse rate. However, where the plume becomes optically thin (effectively semi-transparent) near its edges, heat from the troposphere below makes the templates appear warmer than expected in the stratosphere up to 35 km (> 240 K). In such cases, a colder pattern is being tracked over a warm background, and the 20% coldest pixels are averaged to be more representative of the plume temperature. This approach to

temperature assignment is similar in concept to that proposed by Borde, et al. (2014) where the assignment is being made based on the pixels that are most important for feature tracking.

ERA5 and GNSS-RO temperature profiles are provided in Figure 2b for context, which may not be entirely accurate in the presence of volcanic ash; however, the EBBTs of both the plume and tropospheric clouds broadly follow and cluster near both profiles. Deviations from the profiles are indicative of challenges with temperature-based height assignment, which in general is complicated by inversions, semitransparency, undercooling, temperature assignment uncertainty, and targets with emissivity less than one. Additional confidence in the stereo retrievals is gained by noting that the field of marine stratocumulus (Sc) clouds in the SW quadrant of the mesoscale domain has stereo heights between 500 m and 1.5 km. These are within expectations for such clouds and match well with the NOAA temperature-based cloud top height product for this scene.

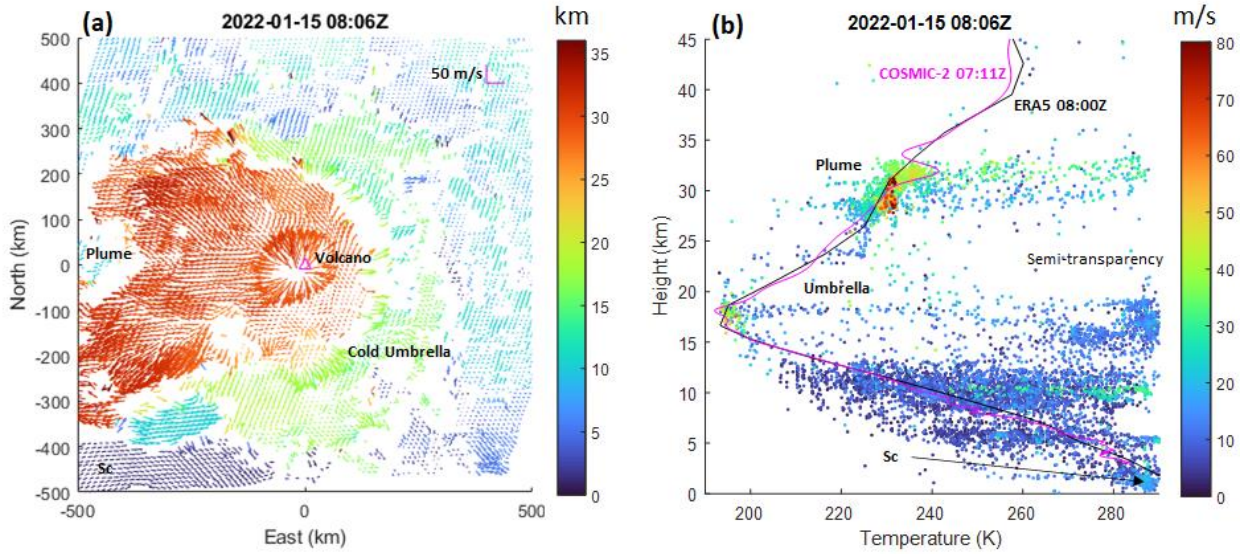

Figure 2. Panel (a) shows the jointly retrieved heights and horizontal advection vectors at their parallax corrected locations centered on the volcano (20.536°S, 175.382°W). The vector scale at the upper right indicates a 50 m s^{-1} wind in each direction. Panel (b) shows the assigned temperatures for each retrieval and the associated advection speed. Temperature profiles from ERA5 at 08:00Z and COSMIC-2 RO at 07:11Z have been added for context.

The 08:06Z scene was selected for Figure 2 as an interesting case because it clearly shows an eruption of volcanic ash overshooting the plume top centered over the marked volcanic site (Global Volcanism Program, 2013). All stereo-winds product files are found in the supplement, along with animations of the IR imagery, height-coded advection fields, and height versus temperature profiles for the complete set (Exhibits S4ff). At 08:41Z, an overshooting plume core reached the upper stratosphere with an EBBT of ~173K, significantly colder than the surrounding stratospheric plume. This cold bubble has an EBBT ~15K colder than the lower umbrella near the tropopause, which can be explained by adiabatic cooling during plume convection (Woods and Self, 1992). Atmospheric gravity waves are also evident in the animations.

The evolution of the mesoscale plume height statistics from 07:06Z to 13:46Z for 15 January 2022 is detailed in Figure 3. At each time, this density plot presents the distribution of retrieved heights. Optically thick parts of the plume at a higher altitude can block the view of elements underneath, which explains the lower number density in the cold umbrella when the upper-level plume has a higher number density. If the upper volcanic plume were a mix of optically thin and thick layers, the height retrieval count profile would indicate an approximate upper-plume thickness of 4-5 km. However, as noted, optically thick parts will obscure material below. From 07:06Z to 10:06Z, the upper volcanic plume obscures the lower cold umbrella, decreasing its retrieval numbers, but as the upper volcanic plume moves out of the mesoscale domain, retrievals increase for the slower evolving cold umbrella. Subsequent activity is seen in the volcanic plume retrieval peaks between 07:00Z and 09:00Z that do not surpass height of the initial eruption, for which earlier plume material has advected out of the mesoscale domain. This interpretation is supported by the animation of the stereo retrievals provided in the supplemental material. Overall, the plume ceiling within the mesoscale domain is observed to fall nearly linearly at a rate of ~1.7 km/h.

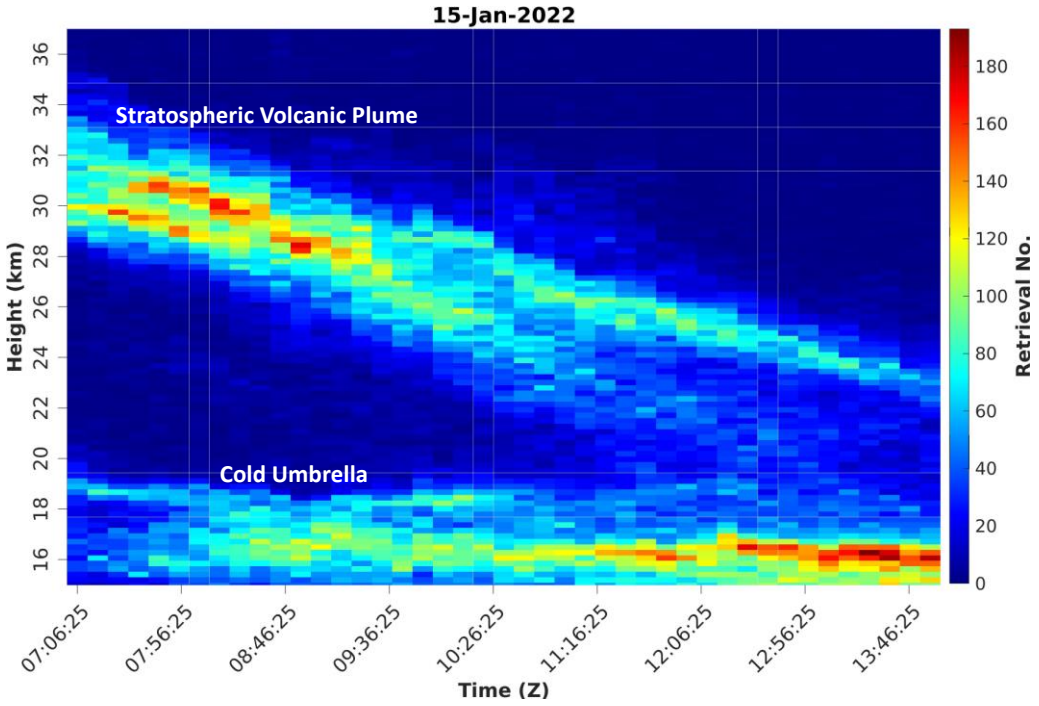

Figure 3. A time series of the distribution of plume height retrievals shows the evolution over a nearly 7-hour period. Advection out of the mesoscale domain and thinning of the higher-level plume causes more of the cold umbrella near the tropopause to be revealed as time progresses.

4.3 Radio Occultation Results

The GNSS-RO technique has been used operationally in numerical weather prediction to provide temperature information in the lower stratosphere and upper troposphere through the bending induced by atmospheric refractivity (Healy et al., 2005). Bending Angle (BA) is the critical parameter used to profile atmospheric variability from GNSS-RO and increases exponentially as the surface approaches. This study uses near real-time data from the

Constellation Observing System for Meteorology, Ionosphere and Climate-2 (COSMIC-2), and Spire under NOAA's Commercial Weather Data Pilot (CWDP) program.

To detect volcano-induced BA perturbations on January 15, we first derive a BA reference profile for the latitude band (15°S to 25°S) using all BA profiles from January 14 and 16. Then, we take the difference between individual profiles from January 15 and the reference BA to find anomalies near the Tonga eruption region. The BA perturbation is measured in percentage from the difference divided by the reference BA. Typically, a BA profile varies within 10% about the reference at heights between 20-40 km.

As shown in Figure 4, two strong BA perturbations are observed around 05:17:40Z (from COSMIC-2) and 05:12:42Z (from Spire), indicating an ~50% deviation from the reference. The top heights of the BA perturbations are approximately 41 km and 38 km, respectively for these cases. The GNSS-RO technique has a relatively good (< 2 km) vertical but poor (~300 km) horizontal resolution. Thus, the bending is sensitive to the refractivity change induced by a large volcanic plume like that of the Tonga eruption. The top of the BA perturbation indicates the first height where the RO line-of-sight encounters the volcanic plume. Starting with the average of the two RO measurements, 39.5 km at 05:15Z, and extrapolating forward with the fall rate of 1.7 km/h (identified in Figure 3) until 07:06Z predicts a maximum plume top of 36.4 km. This agrees with the highest retrievals in the 07:06Z histogram to the expected vertical resolution of the RO observations.

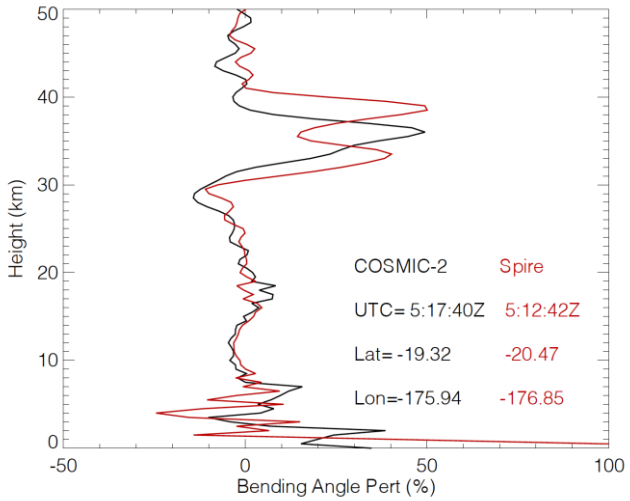

Figure 4. Perturbations of the Bending Angle (BA) profile observed by COSMIC-2 and Spire GNSS-RO from 15 January 2022 with respect to the reference profile. The sharp BA change in the stratosphere indicates the impact of the volcanic plume on radio-wave propagation. The plot indicates the locations and times of the RO profiles.

4 Conclusions

We used GOES-17 and Himawari-8 geostationary satellite imagery to study the 15 January 2022 eruption of the Hunga Tonga-Hunga Ha'apai volcano shortly after 04:00Z. Manually measured parallaxes between near-simultaneous visible images from each satellite and the lengths of shadows cast by the plume provided information about plume structure in the earliest phases of

the eruption. We applied a stereo-winds tracking method starting at 07:06Z to automatically generate a high-density representation of plume advection jointly retrieved with plume height. This powerful method provided a detailed mesoscale description of advection and vertical structure for nearly seven hours every 10 minutes.

Our results show that the Hunga Tonga-Hunga Ha'apai volcano ejected material as high as 55 km, with a substantial amount of material injected above 30 km. Such peak altitudes exceed the maximum column altitudes of 40 km reported for the 1991 Mount Pinatubo eruption by Holasek et al. (1996). As the eruption progressed and later died down, advection carried much of the injected stratospheric plume outside the mesoscale domain studied. The plume remaining in the mesoscale domain would have thinned or collapsed to render it untrackable in the IR imagery. Our analysis of GNSS-RO bending angles confirms that material was lofted between 30 km and 40 km approximately one hour after the initial eruption.

Acknowledgments

The authors thank Andrew Heidinger and Jaime Daniels, at NOAA, and Steve Wanzong, at the University of Wisconsin, for valuable discussions.

The work of J. Carr was supported by NASA Goddard Space Flight Center under the NNG17HP01C contract through Support for Atmospheres, Modeling, and Data Assimilation (SAMDA). The work of Á. Horváth was supported by Deutsche Forschungsgemeinschaft (DFG) project VolImpact/VolPlume (contract BU 2253/7-1). The work of D. Wu and M. Friberg was supported by NASA's Terra project and Sun-Climate research. Resources supporting the automated stereo wind retrievals were provided by the NASA High-End Computing (HEC) Program through the NASA Center for Climate Simulation (NCCS) at Goddard Space Flight Center.

Competing interests

The authors declare that they have no conflict of interest.

Open Research

All mesoscale stereo retrievals are included in the supplementary material submitted with this paper. GOES-17, Himawari-8, and GNSS-RO are publicly available at https://class.noaa.gov, https://registry.opendata.aws/collab/noaa/, and https://cdaac-www.cosmic.ucar.edu/. Stereo method for manual photogrammetry: Fuji (Schindelin, et al. 2012).

References

Borde, R., M. Doutriaux-Boucher, G. Dew & M. Carranza (2014). A Direct Link between Feature Tracking and Height Assignment of Operational EUMETSAT Atmospheric Motion

Vectors, *Journal of Atmospheric and Oceanic Technology*, *31*, 33–46. https://doi.org/10.1175/JTECH-D-13-00126.1.

Carr, J. L., D. L. Wu, J. Daniels, M. D. Friberg, W. Bresky, & H. Madani. (2020). GEO–GEO Stereo-Tracking of Atmospheric Motion Vectors (AMVs) from the Geostationary Ring. *Remote Sensing*, *12*, no. 22: 3779. https://doi.org/10.3390/rs12223779.

Global Volcanism Program (2013). Hunga Tonga-Hunga Ha'apai (243040) in Volcanoes of the World, v. 4.10.4 (09 Dec 2021). Venzke, E (ed.). Smithsonian Institution. Downloaded 28 Jan 2022 (https://volcano.si.edu/volcano.cfm?vn=243040). https://doi.org/10.5479/si.GVP.VOTW4-2013.

Healy, S. B., A. M. Jupp, & C. Marquardt (2005). Forecast impact experiment with GPS radio occultation measurements, *Geophysical Research Letters*, *32*, L03804. https://doi.org/10.1029/2004GL020806.

Holasek, R. E., S. Self, & A. W. Woods (1996), Satellite observations and interpretation of the 1991 Mount Pinatubo eruption plumes, *Journal of Geophysical Research*, *101*(B12), 27635–27655. https://doi.org/10.1029/96JB01179.

Horváth, Á., J. L. Carr, O. A. Girina, D. L. Wu, A. A. Bril, A. A. Mazurov, D. V. Melnikov, G. A. Hoshyaripour, & S. A. Buehler (2021). Geometric estimation of volcanic eruption column height from GOES-R near-limb imagery – Part 1: Methodology, *Atmospheric Chemistry and Physics*, *21*, 12189–12206. https://doi.org/10.5194/acp-21-12189-2021, 2021.

Horváth, Á., O. A. Girina, J. L. Carr, D. L. Wu, A. A. Bril, A. A. Mazurov, D. V. Melnikov, G. A. Hoshyaripour, & S. A. Buehler (2021). Geometric estimation of volcanic eruption column height from GOES-R near-limb imagery – Part 2: Case studies, *Atmospheric Chemistry and Physics*, *21*, 12207–12226. https://doi.org/10.5194/acp-21-12207-2021, 2021.

Merucci, L., K. Zakšek, E. Carboni, & S. Corradini (2016). Stereoscopic Estimation of Volcanic Ash Cloud-Top Height from Two Geostationary Satellites, *Remote Sensing*, *8*, no. 3: 206. https://doi.org/10.3390/rs8030206.

Prata, A. J., & I. F. Grant (2001). Determination of mass loadings and plume heights of volcanic ash clouds from satellite data, CSIRO Atmospheric Research Technical Paper no. 48, available at: http://www.cmar.csiro.au/e-print/open/prata_2001a.pdf (last access: 28 January 2022).

Schindelin, J., I. Arganda-Carreras, E. Frise, V. Kaynig, M. Longair, T. Pietzsch, S. Preibisch, C. Rueden, S. Saalfeld, B. Schmid, J. Y. Tinevez, D. J. White, V. Hartenstein, K. Eliceiri, P. Tomancak, & A. Cardona (2012), Fiji: an open-source platform for biological-image analysis, *Nature Methods*, *9*, 676–682. https://doi.org/10.1038/nmeth.2019.

Woods, A. & S. Self (1992). Thermal disequilibrium at the top of volcanic clouds and its effect on estimates of the column height. *Nature*, *355*, 628–630. https://doi.org/10.1038/355628a0.